Dynamically stiffened matrix promotes malignant transformation of mammary epithelial cells via collective mechanical signaling

Matthew G. Ondeck[a,1,2], Aditya Kumar[b,1], Jesse K. Placone[b,1], Christopher M. Plunkett[b], Bibiana F. Matte[b,c], Kirsten C. Wong[b], Laurent Fattet[d], Jing Yang[d,e,f], and Adam J. Engler[a,b,e,g,3]

[a]Material Science Program, University of California, San Diego, La Jolla, CA 92093; [b]Department of Bioengineering, University of California, San Diego, La Jolla, CA 92093; [c]Department of Oral Pathology, Federal University of Rio Grande do Sul, Porto Alegre, RS 90040-060, Brazil; [d]Department of Pharmacology, University of California, San Diego, La Jolla, CA 92093; [e]Biomedical Sciences Program, University of California, San Diego, La Jolla, CA 92093; [f]Department of Pediatrics, University of California, San Diego, La Jolla, CA 92093; and [g]Sanford Consortium for Regenerative Medicine, La Jolla, CA 92037

Edited by David A. Weitz, Harvard University, Cambridge, MA, and approved January 15, 2019 (received for review August 17, 2018)

Breast cancer development is associated with increasing tissue stiffness over years. To more accurately mimic the onset of gradual matrix stiffening, which is not feasible with conventional static hydrogels, mammary epithelial cells (MECs) were cultured on methacrylated hyaluronic acid hydrogels whose stiffness can be dynamically modulated from "normal" (<150 Pascals) to "malignant" (>3,000 Pascals) via two-stage polymerization. MECs form and remain as spheroids, but begin to lose epithelial characteristics and gain mesenchymal morphology upon matrix stiffening. However, both the degree of matrix stiffening and culture time before stiffening play important roles in regulating this conversion as, in both cases, a subset of mammary spheroids remained insensitive to local matrix stiffness. This conversion depended neither on colony size nor cell density, and MECs did not exhibit "memory" of prior niche when serially cultured through cycles of compliant and stiff matrices. Instead, the transcription factor Twist1, transforming growth factor β (TGFβ), and YAP activation appeared to modulate stiffness-mediated signaling; when stiffness-mediated signals were blocked, collective MEC phenotypes were reduced in favor of single MECs migrating away from spheroids. These data indicate a more complex interplay of time-dependent stiffness signaling, spheroid structure, and soluble cues that regulates MEC plasticity than suggested by previous models.

mammary | epithelial-to-mesenchymal transition | hydrogel | hyaluronic acid

Tissue remodeling results in part from mechanical, structural, and compositional changes to the extracellular matrix (ECM)—the scaffold that surrounds and separates cells. Significant focus over the last decade has illustrated how one such property—ECM stiffness—effects a range of cell behaviors from migration (1) to alignment and morphology (2–4) to differentiation (5–7). However, the remodeling that induces these changes can occur for a number of reasons: For mammary cancers, tumors "feel" stiffer during manual palpation (8) in part from increased ECM expression and cross-linking (9, 10) as well as changes in protein composition (11, 12). This dynamic tumor microenvironment is established by tumor and stromal cells and their soluble factors (13–15), which evolve as the tumor progresses over months to years (8). Animal models largely recapitulate the dynamics of human tumors, e.g., stiffening by lysyl oxidase-mediated cross-linking (9), but they remain exceedingly complex. Reductionist approaches using biological and synthetic materials have only recently been available to systematically modulate physical properties over a pathologically relevant range. These materials re-create the classic mesenchymal transformation of mammary epithelial cells (MECs) via changes in stromal stiffness (16, 17). However, these materials, especially synthetic ones, often cannot be remodeled by cells in vitro and remain static with time, unlike highly dynamic mammary tissue that undergoes a 10- to 20-fold stiffening during tumor progression (16).

Recent material advances have created dynamic or "on-demand" systems where cross-linking is temporally regulated to achieve continuous or step-wise cross-linking or degradation that more closely resembles in vivo tissue dynamics. Systems often rely on thermal-activated or photo-activated, pH, enzymatic, or diffusion-based mechanisms (18); for example, gold nanorod-carrying liposomes can be heated past their transition temperature to induce rupture and, when loaded with calcium, form additional alginate cross-links (19). Large thermal changes may be detrimental to cells, so light, which can be precisely controlled over space and time, serves as an alternative. Both UV light (UV) activated cross-linking via radical polymerization (20, 21) or degradation via *o*-nitro benzyl groups (22) have been used to modulate cell behavior, finding that stem cells can dynamically modulate their lineage initially (21) but commit after long-term culture (5, 23). Similar memory may exist in cancer cells (24), prompting the question of whether MECs, which form hollow 3D structures called acini in vivo, exhibit single or collective cell behavior when cultured in dynamically stiffening materials. These systems also better mimic how the microenvironment is

Significance

Gradual stiffening of the native extracellular matrix has been implicated in promoting breast cancer progression through stiffness-mediated signaling. Herein, we probe mammary epithelial cell responses to substrate stiffness with a dynamically stiffened hydrogel, enabling investigation of how the change in substrate stiffness impacts collective cell behaviors. We demonstrate that signaling pathways, both paracrine and mechanosensing, impact mammary epithelial cell response to stiffening and act in concert to drive epithelial-mesenchymal plasticity. Interestingly, previous static stiffness hydrogel studies did not observe this interplay of signaling, highlighting the need for dynamic materials to recapitulate disease development. These responses can also be inhibited, individually and together, demonstrating how dynamic stiffening drives cancer progression.

Author contributions: M.G.O., A.K., J.K.P., C.M.P., J.Y., and A.J.E. designed research; M.G.O., A.K., J.K.P., C.M.P., B.F.M., K.C.W., and L.F. performed research; J.Y. and A.J.E. contributed new reagents/analytic tools; M.G.O., A.K., J.K.P., C.M.P., B.F.M., and K.C.W. analyzed data; and M.G.O., A.K., J.K.P., C.M.P., B.F.M., J.Y., and A.J.E. wrote the paper.

The authors declare no conflict of interest.

This article is a PNAS Direct Submission.

Published under the PNAS license.

[1]M.G.O., A.K., and J.K.P. contributed equally to this work.

[2]Present address: Center for Devices and Radiological Health, Food and Drug Administration, Silver Spring, MD 20993.

[3]To whom correspondence should be addressed. Email: aengler@ucsd.edu.

This article contains supporting information online at www.pnas.org/lookup/suppl/doi:10.1073/pnas.1814204116/-/DCSupplemental.

Published online February 12, 2019.

Downloaded at Palestinian Territory, occupied on November 25, 2021

www.manaraa.com

modified over time with tumors versus static materials, enabling us to additionally determine when and to what extent mammary spheroids, i.e., precursors to acini, are sensitive to ECM stiffness.

Results

Methacrylated Hyaluronic Acid Hydrogels Recapitulate Mammary Morphogenesis. Dynamic changes in matrix stiffness—not just stiffness itself (16)—may play a pivotal role in regulating epithelial to mesenchymal transition (EMT), a process where MECs adopt a more mesenchymal-like phenotype punctuated by expression of canonical mesenchymal transcription factors including Twist1 (25). To examine the collective responses of 3D mammary spheroids to stiffening, we adopted a material-based strategy where the methacrylated glycosaminoglycan hyaluronic acid (MeHA) would be partially cross-linked, cells seeded on its collagen-functionalized surface, and Matrigel overlaid on top (*SI Appendix*, Fig. S1 *A–D*), consistent with previous methods that used static polyacrylamide (PA) (16). MeHA has a stiffness range that spans normal to pathologically stiff (Fig. 1*A*) and could be modulated by the methacrylation substitution ratio, free radical donor concentration, and UV exposure time (26); moreover, its mechanics are predominantly elastic rather than viscous (*SI Appendix*, Fig. S1*E*). Collagen can be covalently attached to MeHA (Fig. 1*B*) to a degree similar to PA hydrogels as assessed by how tethered the matrix protein is to the substrate (27). Initial MEC attachment did not vary as a function of stiffness or substrate (Fig. 1*C*) and MeHA,

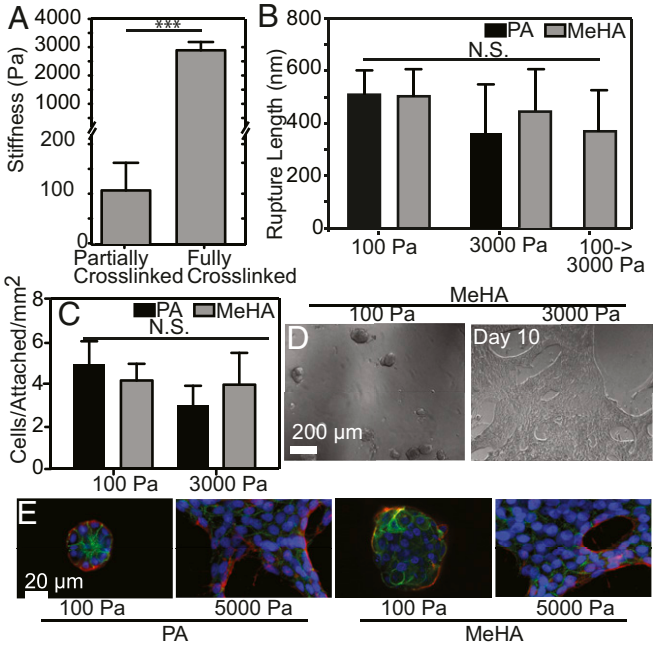

Fig. 1. Tunable MeHA hydrogels have similar properties to PA hydrogels. (*A*) MeHA stiffness is plotted for hydrogels that were cross-linked in a two-stage process (26). Data represent mean ± SD in triplicate ($n > 100$ measurements per bar). ***$P < 10^{-3}$ from an unpaired Student t test. (*B*) Type I collagen attachment is shown by rupture length of the tether pulled off of the surface as in Wen et al. (27) to assess protein-hydrogel coupling. No statistical difference by two-way ANOVA was found between 100 Pa and 3,000 Pa hydrogels fabricated using MeHA or PA as well as MeHA hydrogels that were stiffened using the two-stage process ($n > 100$ measurements over three independent gels per bar). (*C*) Initial MEC attachment is plotted as a function of stiffness or substrate. No statistical difference by two-way ANOVA was found ($n = 3$ hydrogels containing over 50 cells per bar). (*D*) Phase images demonstrating MCF10A cell response on 100 and 3,000 Pa MeHA substrates. (Scale bar: 200 μm.) (*E*) Fluorescent images of E-cadherin (green), Laminin V (red), and nuclei (blue) for both 100 and 3,000 Pa substrates made using either polyacrylamide (PA) or MeHA (16, 17). N.S., not significant.

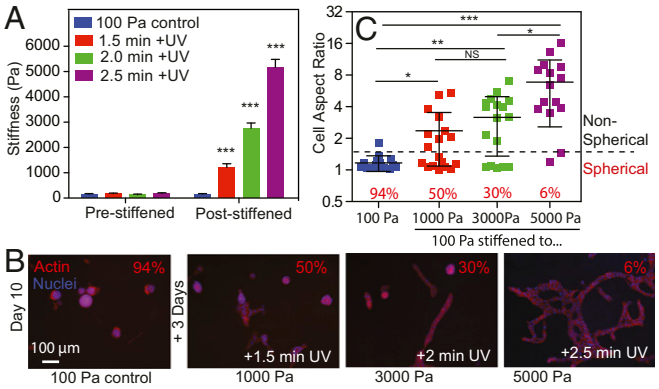

Fig. 2. MeHA substrates have tunable stiffness to interrogate MEC response to dynamic stiffening. (*A*) Hydrogel stiffness was measured using AFM for substrates after the initial polymerization step (prestiffened) and then after the second polymerization step (poststiffened). Each color corresponds to a different UV duration in the presence of the Irgacure 2959 ($n = 6$ hydrogels with >20 measurements per gel for each bar). ***$P < 10^{-3}$ from a paired Student t test between the prestiffened and poststiffened states of each substrate. (*B*) MECs were cultured as indicated and stained for actin (red) and nuclei (blue). (*C*) Cell aspect ratio is plotted with each color corresponding to the stiffening regiment in *A*. The dashed line at 1.5 indicates an approximate transition point from spherical to nonspherical morphology. The percentage of data below the transition is shown, indicating the fraction of the population that remains spherical. *$P < 0.05$, **$P < 1 \times 10^{-2}$, and ***$P < 1 \times 10^{-3}$ from an unpaired Student t test ($n > 15$ spheroids per condition). N.S., not significant.

stiffened only to initially polymerize it, yielded MEC responses consistent with previous results on PA hydrogels (16); pathologically stiff cultures induce EMT, whereas physiological compliant cultures do not (Fig. 1 *D* and *E*).

Spheroid EMT Depends on Magnitude and Timing of Substrate Stiffening. Via static culture, single MECs undergo EMT and form a layer of mesenchymal cells above 400 Pa or >twofold above normal ECM stiffness (16). To determine to what extent MECs are sensitive collectively to ECM stiffness as spheroids, single cells were cultured on 100-Pa MeHA hydrogels to form mammary spheroids and then stiffened to varying degrees after 10 d (Fig. 2*A*). Stiffening up to 3,000 Pa requires the presence of both a free radical donor and UV (*SI Appendix*, Fig. S2) up to 2.5 min, which was not sufficient to induce DNA damage pathways, e.g., p53 activation (*SI Appendix*, Fig. S3); these data suggest that MEC responses are stiffness-mediated and not the result of MeHA polymerization chemistry. After substrates were stiffened to reach 1,000–5,000 Pa (Fig. 2*A*), we found that collective MEC responses were still stiffness-dependent; fewer maintained their spheroid morphology on 5,000 vs. 1,000 Pa hydrogels, often exhibiting significant migration away from the original spheroid (Fig. 2*B*). However, cell responses were notably heterogeneous at intermediate stiffness; despite 10-fold change in stiffness, 50% of spheroids maintained their morphology when MeHA hydrogels were stiffened from 100 to 1,000 Pa. Conversely, relatively few spheroids remained when MeHA was stiffened to pathological stiffness (Fig. 2*C*). To confirm these results, we additionally tested the mouse epithelial cell line, Eph4Ras, and found similar results to human MCF10A cells (*SI Appendix*, Fig. S4). Cell responses also appear to be sensitive to any change in matrix stiffness, whether performed as a single or two-step stiffening. When stiffened over 2 d, first to the stiffness where single cells were found to be responsive, e.g., 600 Pa (16, 28), and then to pathological stiffness, we observed analogous resistance to the change in stiffness on mammary spheroid morphology (*SI Appendix*, Fig. S5). These data suggest that the heterogeneity of tumor progression may be due in part to different sensitivities of a collective MEC response to stroma stiffness changes.

Downloaded at Palestinian Territory, occupied on November 25, 2021

www.manaraa.com

To examine the onset of collective stiffness sensitivity, we next varied MEC culture time before stiffening MeHA substrates to the same degree (Fig. 3*A*). With increased culture time on physiological stiffness, MECs formed spheroids (Fig. 3*B*, *Left*) whereas MECs on pathologically stiff substrates exhibited spreading, and morphological changes indicative of EMT-like behavior as early as 2 d in culture (Fig. 3*B*, *Right*). However, when stiffened to 3,000 Pa after a variable amount of preculture time at 100 Pa, we found that collective MEC responses became heterogeneous after 8–10 d of preculture; ∼10–20% of spheroids did not respond to stiffening by exhibiting EMT-like behavior (Fig. 3*B*, *Middle* and Fig. 3*C*), suggesting that after sufficient time in culture, they may have matured to the point where collective sensing among cells within the spheroid could override mechanotransductive signals that would induce EMT for those cells in contact with the MeHA (17). However, MECs proliferate (11) and acini hollow (29) as they mature, so the number of cells present in spheroid may regulate their collective sensing. To produce spheroids of consistent size, MECs were preclustered at different densities using Aggrewell plates. After seeding overnight on MeHA, hydrogels were stiffened and spheroids cultured for up to 5 d (Fig. 4*A*). However, the behavior appeared independent of cell density as it did not affect the propensity of

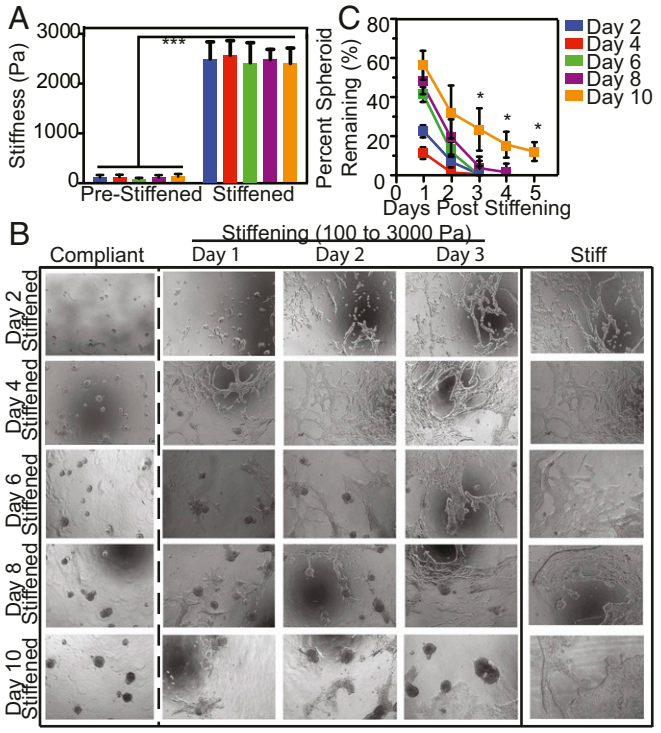

Fig. 3. Dynamically stiffened MeHA substrates influence MEC stiffness response. (*A*) On culture days 2, 4, 6, 8, and 10 on 100 Pa substrates, samples were stiffened to ∼3,000 Pa. Data represent mean ± SD for polymerization from first batch of MeHA ($n = 6$ hydrogels with >100 measurements per bar). $***P < 10^{-3}$ from an unpaired Student *t* test. (*B*) Representative brightfield images of MECs cultured on MeHA substrates with variable times for stiffening corresponding to *A* and indicated by row (middle columns); total culture time for dynamically stiffened gels are indicated for each row plus the time indicated by each column. For reference, MECs cultured on substrates with stiffness of 100 Pa (*Left*) and 3,000 Pa (*Right*) are shown with each row corresponding to the indicated culture day. (*C*) Quantification of the percent spheroids remaining as a function of the days after stiffening. Data are sorted by preculture time ($n = 2$ biological replicates with ≥2 gels with 80–341 spheroids measured per condition; for 8 d before culture, n = 1 biological replicate with four gels with 70–135 spheroids measured per gel). $****P < 1 \times 10^{-4}$ for time after stiffening and $***P < 1 \times 10^{-3}$ for stiffening day from a two-way ANOVA with $*P < 0.05$ for Tukey's post hoc analysis versus other individual conditions.

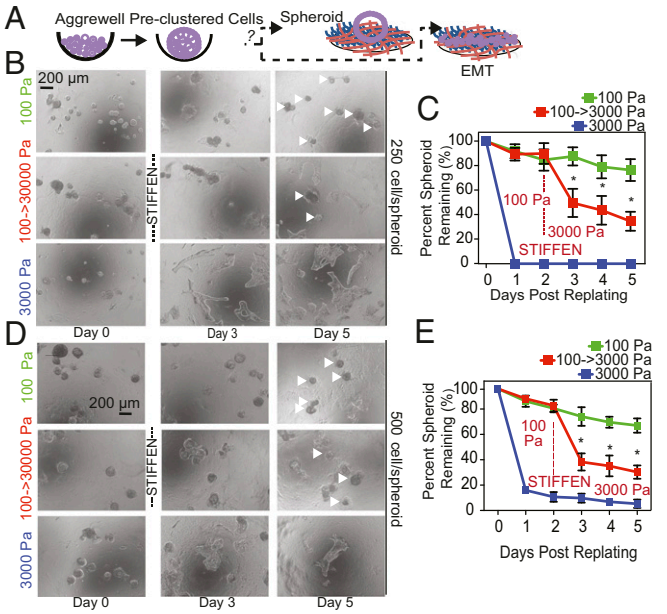

Fig. 4. Ability of MECs to respond to stiffness-mediated changes is size independent. (*A*) Schematic shows how aggrewell plates were used to precluster cells before seeding onto 100 and 3,000 Pa substrates to investigate the dependence on spheroid size or maturity. (*B* and *D*) Spheroids made with 250 and 500 cells, respectively, were seeded onto 100 and 3,000 Pa substrates, and selected 100 Pa hydrogels were stiffened at day 2. Images show resulting morphology at indicated days. White arrowheads denote the spheroids remaining on substrates 5 d after plating. (*C* and *E*) The percent spheroids remaining are shown as a function of days after replating with the day of stiffening indicated for 250 and 500 cells per spheroid, respectively. $*P < 0.05$ for Tukey's post hoc analysis versus other conditions ($n =$ 2 biological replicates containing 33–67 spheroids or EMT cluster per condition for each time point).

MECs to respond to stiffness; indeed, responses were primarily controlled by stiffness. When MeHA was stiffened, we further observed a decrease in spheroids in favor of MECs undergoing EMT-like changes (Fig. 4 *B*–*E*), although we again observed that a subset of spheroids is insensitive to stiffening (Fig. 4 *B* and *D*, *Middle*, arrowheads). Together, these data suggest that collective MEC responses to stroma stiffness changes are heterogeneous.

Stiffening-Induced EMT Is Not a Cell Autonomous Process but Is Augmented by Paracrine Signaling. Single MECs have been suggested to have memory of their previous niche (24), and given the heterogeneous responses of spheroids after stiffening, we next asked if mammary spheroids would exhibit memory. Mammary spheroids were cultured on stiffened hydrogels as in Fig. 3 for 10 d (labeled as 1°), and remaining spheroids were separated from spread cells using a differential typsinization method (*SI Appendix*, Fig. S6). The separated spheroids and spread cell populations were then reseeded on MeHA substrates that were compliant, stiffened, or stiff (labeled as 2°) to assess whether response was cell autonomous (Fig. 5*A*). When spheroids were plated onto the secondary hydrogel without stiffening, cells remained spherical, but when plated onto stiff substrates, most spheroids exhibited EMT-like changes (Fig. 5 *B* and *C*, green vs. blue). When plated on stiffened 2° hydrogels, nearly all spheroids were maintained until stiffening, at which point the population became heterogeneous again (Fig. 5 *B* and *C*, red). Conversely, when spread MECs were plated onto stiff 2° hydrogels, cells remained spread (Fig. 5 *D* and *E*, blue), but for both compliant and stiffened MeHA, MECs formed spheroids, which became heterogeneous only when MeHA was stiffened during the 2° screen (Fig. 5 *D* and *E*, green vs. red). To more closely assess phenotype resulting from spheroids and spread cells in the 2° hydrogel, we examined E-cadherin localization and

Downloaded at Palestinian Territory, occupied on November 25, 2021
www.manaraa.com

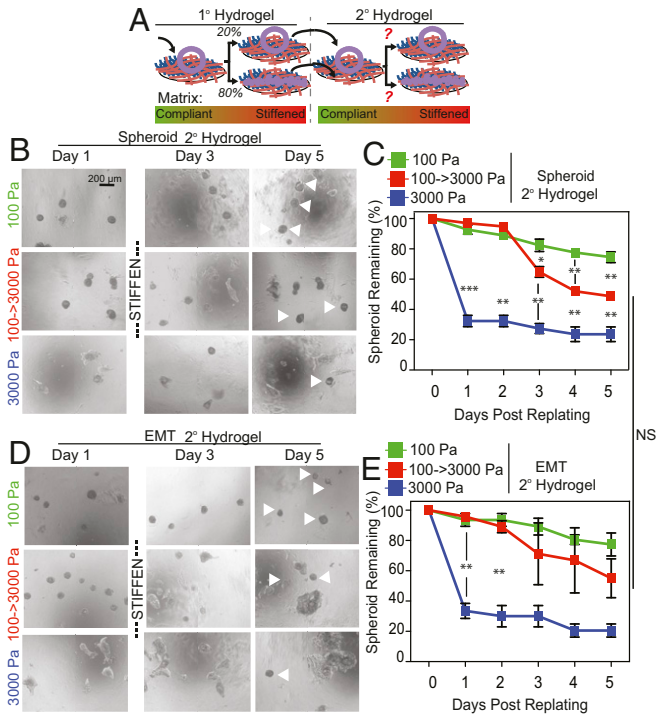

Fig. 5. MEC spreading is not cell autonomous. (*A*) Schematic depicting 1° and 2° screens of spheroids that were cultured on stiffened hydrogels during the 1° screen. Cells undergoing EMT were separated from spheroids using the method in *SI Appendix*, Fig. S6 and replated in the 2° screen on 100 Pa, 3,000 Pa, or a substrate stiffened from 100 to 3,000 Pa. (*B* and *D*) Representative images up to day 5 after replating from the 2° screen of cells isolated from spheroid and EMT regions of the primary screen, respectively. For substrates that were stiffened (*Middle*), timing of matrix stiffening is noted. White arrowheads denote the spheroids remaining on substrates 5 d after plating. (*C* and *E*) The percent spheroids remaining are shown as a function of days after replating with the day of stiffening indicated for cells isolated from spheroids and EMT regions of the primary screen, respectively ($n = 2$ biological replicates containing 10–71 spheroid or EMT cluster per condition for each time point). $^{*}P < 0.05$, $^{**}P < 1 \times 10^{-2}$, and $^{***}P < 1 \times 10^{-3}$ for Tukey's post hoc analysis versus other conditions at the same time point. Two-way ANOVA was not significant (NS) for effect of EMT vs. spheroid.

found that regardless of input MEC type (spherical or spread), spheroids on compliant MeHA had peripheral E-cadherin localization and typically exhibited hollow centers (*SI Appendix*, Figs. S7 and S8, *Top*). Surprisingly, spread cells on stiff MeHA had similar peripheral E-cadherin localization although they lacked polarized orientation (*SI Appendix*, Figs. S7 and S8, *Bottom*); both results were present when MeHA was stiffened (*SI Appendix*, Figs. S7 and S8, *Middle*). Since both cell populations adapted to their local microenvironment and responded to stiffening—consistent with the heterogeneous response observed in Fig. 3—which suggests that cell decisions are not autonomous and rather involve transient and collective signaling among cells within the spheroids or spreading MECs.

Heterogeneous Stiffening-Mediated Responses Occur via TGFβ and YAP Signaling. E-cadherin expression and localization suggests that paracrine signaling may augment collective behavior. TGFβ is a common soluble factor that affects EMT (25), so exogenous TGFβ was added to culture media of spheroids from Fig. 5 plated onto compliant, stiffened, and stiff substrates to determine to what extent a paracrine signal could influence collective stiffness sensing. In all conditions, the number of spheroids remaining was greatly reduced, with progressive loss occurring even after stiffening as well as on compliant substrates absent any stiffness signal (*SI Appendix*, Fig. S9). Unlike in the absence of TGFβ on stiff MeHA where E-cadherin expression was lower but still localized, we observed complete loss of E-cadherin by day 5 in the presence of TGFβ on stiff MeHA (*SI Appendix*, Fig. S10).

Given that exogenous TGFβ induced increased spreading on all conditions but especially on stiffened MeHA, we next assessed stiffness-mediated localization of SMAD2/3, a signaling complex immediately downstream of TGFβ receptor, and Twist1, a basic helix-loop-helix transcription factor associated with stiffness-mediated EMT (17, 25). Both SMAD and Twist1 nuclear localized on pathologically stiff (Fig. 6*A*, filled arrowheads) but not physiologically compliant matrices (open arrowheads) (Fig. 6 *A* and *B*). For stiffened hydrogels, both spherical and spread cell subpopulations exhibited heterogeneous distributions of localized (filled arrowheads) and nonlocalized (open arrowheads) SMAD and Twist1 (Fig. 6 *C* and *D*). When cells on stiff and stiffened conditions nuclear-localized SMAD, we observed its phosphorylation (*SI Appendix*, Fig. S11), indicating a transcriptionally active and stiffness-responsive SMAD complex. To decouple TGFβ signaling from stiffening-induced responses, 10 μM Galunisertib, a TGFβ receptor inhibitor, was added to culture media of spheroids on compliant substrates that were subsequently stiffened. Although inhibition prevented SMAD2/3 nuclear localization (*SI Appendix*, Fig. S12 *A* and *B*), a subset of cells still left the spheroids, spread, and became motile (*SI Appendix*, Fig. S12*C*). However, this population was significantly smaller and less migratory for Galunisertib-treated cells (*SI Appendix*, Fig. S12 *D* and *E*). These data suggest that stiffening on MeHA substrates induces a collective paracrine cell response via TGFβ signaling in concert with other mechanosensitive pathways.

To determine the underlying mechanism for non-SMAD/Twist spread cells when exposed to dynamic matrix stiffness, we assessed the localization and activity of the mechanosensitive transcription activator Yes-associated protein 1 (YAP) (30) which has been recently implicated in several metastatic cascades (24, 31). As with Twist1, YAP nuclear localization was observed on stiff hydrogels but not compliant (Fig. 7*A*, *Bottom*). However, on stiffened hydrogels, 29% of cells had nuclear-localized YAP but not SMAD (Fig. 7 *C* and *D*); conversely, only 8% of cells were Twist1 but not SMAD2/3 positive (Fig. 6*D*). Furthermore,

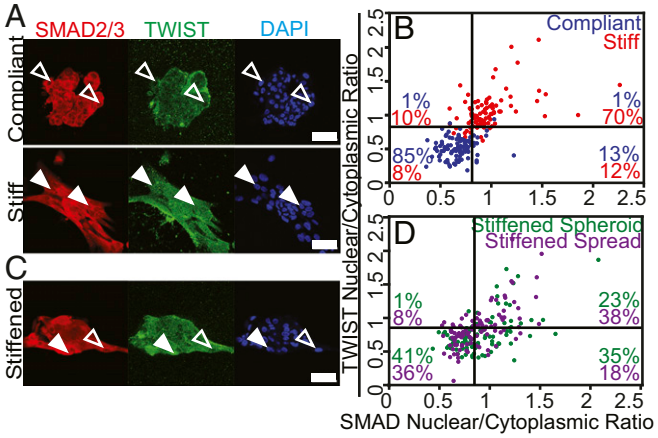

Fig. 6. TWIST and SMAD localization in spherical and spread MECs. (*A*) TWIST (green) and SMAD2/3 (red) immunofluorescent imaging of MECs on compliant and stiff substrates. Images show cells that have cytoplasmic localization of TWIST and SMAD (open arrowheads) on compliant gels and nuclear localization (filled arrowheads) on stiff gels. (*B*) Plot of the nuclear to cytoplasmic intensity ratio for Twist and SMAD2/3 for the indicated conditions ($n = 100$ cells). Lines delineate separation of data between compliant and stiff. (*C*) TWIST and SMAD2/3 immunofluorescent imaging for MECs on stiffened substrates. Arrowheads indicate cells that are cytoplasmic or nuclear localized. (*D*) Plot of the nuclear to cytoplasmic intensity ratio for Twist and SMAD on stiffened substrates ($n = 100$ cells). The lines from *B* were used to identify cells as either positive or negative for the markers.

Downloaded at Palestinian Territory, occupied on November 25, 2021
APPLIED BIOLOGICAL SCIENCES
ENGINEERING
www.manaraa.com

TGFβ receptor inhibition resulted in clear stratification of the spherical and spread, motile subpopulations into YAP nonlocalized and YAP localized groups, respectively (*SI Appendix*, Fig. S13 *A* and *B*), suggesting a role for YAP in initiating non-TGFβ–mediated spreading. To understand the role of YAP activity in the spread cell phenotype, we inhibited its activity with Verteporfin, a small molecule that reduces endogenous YAP expression and prevents nuclear activation (32). While Verteporfin reduced YAP nuclear expression, it did not inhibit EMT-like morphological changes on stiff hydrogels (*SI Appendix*, Fig. S14). Interestingly, YAP inhibition on stiffened gels resulted in a significant reduction of migration similar to TGFβ receptor inhibition (*SI Appendix*, Fig. S15). However, while YAP or TGFβ receptor inhibition alone resulted in significantly fewer spread and motile cells per spheroid, dual inhibition provided the greatest overall reduction in the total number of spread, motile cells (Fig. 8 *A* and *B*). Together these data suggest that collective signaling throughout the spheroid may be sensed through a combination of both paracrine signaling via TGF-β/SMAD and mechanical signaling via YAP localization, and that when jointly inhibited, spheroids composed of MECs give rise to significantly fewer cells capable of spreading and migrating into the surrounding stroma (Fig. 8*C*).

Discussion

MeHA-based hydrogels recapitulate mammary morphogenesis in vitro as classic, static biomaterial systems do (16, 17), but its ability to be dynamically stiffened to mimic in vivo pathogenesis provides a tool to elucidate events and signaling not otherwise observable under static conditions, e.g., dual TGF-β/SMAD and YAP collective signaling versus that previously observed with Twist and integrins. Here, we show that preculture on compliant substrates resulted in a population of spheroids that were partially resistant to stiffness-mediated spreading. MEC response depended on not only the magnitude of dynamic stiffening, but also the timing of substrate stiffening. We also demonstrated that the MECs did not exhibit memory-like behavior but rather that stiffness-dependent MEC responses at the local cell level were modulated by TGFβ and YAP signaling; augmenting or inhibiting this signal induced collective EMT or caused stiffness-sensitive

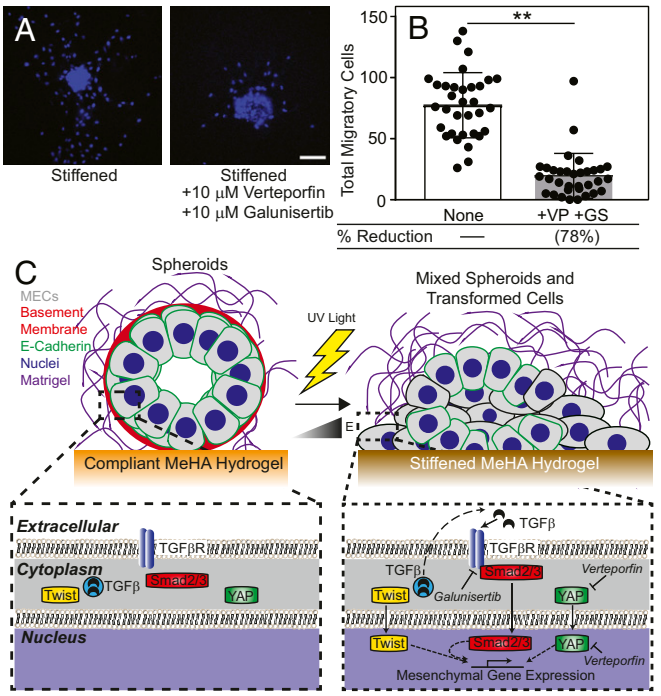

Fig. 8. YAP and SMAD inhibition reduces number of spread cells on stiffened gels. (*A*) Images demonstrating spread cells on stiffened substrates and cells treated with Galunisertib and Verteporfin. (*B*) Total number of spread cells per spheroid was plotted for untreated and treated cells. $*P < 0.05$, $**P < 1 \times 10^{-2}$, and $***P < 1 \times 10^{-3}$ for Tukey's post hoc analysis. (*C*) Mechanism describing inhibition of YAP and SMAD nuclear localization on MECs spreading.

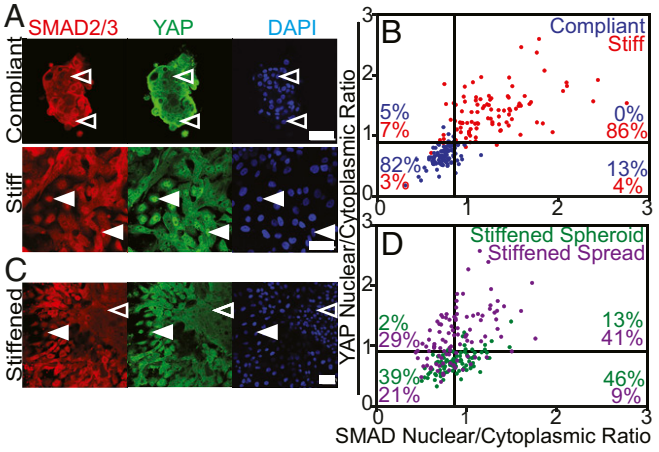

Fig. 7. YAP and SMAD localization in spherical and spread MECs. (*A*) YAP (green) and SMAD2/3 (red) immunofluorescent imaging of MECs on compliant and stiff substrates. Images show cells that have cytoplasmic localization of YAP and SMAD2/3 (open arrowheads) on compliant gels and nuclear localization (filled arrowheads) on stiff gels. (*B*) Plot of the nuclear to cytoplasmic intensity ratio for YAP and SMAD2/3 for the indicated conditions ($n = 100$ cells). Lines delineate separation of data between compliant and stiff. (*C*) YAP and SMAD2/3 immunofluorescent imaging for MECs on stiffened substrates. Arrowheads indicate cells that are cytoplasmic or nuclear localized. (*D*) Plot of the nuclear to cytoplasmic intensity ratio for YAP and SMAD2/3 on stiffened substrates ($n = 100$ cells). The lines from *B* were used to identify cells as either positive or negative for the markers.

cells to respond and migrate individually, respectively. These results implicate a more complex interplay of paracrine and time-dependent stiffness-mediated cellular changes leading to EMT than suggested by previous static models (16, 17) but in line with in vivo systems (9, 14, 33). Similar complexities have been observed in the context of other matrix properties as well as more complex mechanical behaviors, i.e., stress relaxation (34). Thus, our data and the field suggest that a broader biomaterials exploration is required; for example, how does mechanical signaling dynamically change in conjunction with topographic (35), adhesive (36), or porosity (37) changes? Even beyond MECs, dynamic stiffening may control cell fate, e.g., cardiomyocyte differentiation, by turning on and off mechanically sensitive pathways over time (38). Clearly this phenomenon of dynamic biomaterial property regulation of cell fate—from stem cells to cancer—warrants increasing attention from the biomedical engineering community.

Methods

MeHA Hydrogel Formulation. Twelve-millimeter glass coverslips were cleaned via sonication in 70% EtOH for 10 min followed by DI H_2O for 10 min. Coverslips were dried and treated with 0.1 mg/mL poly-D-lysine (70–150 kDa, P6407; Sigma-Aldrich) for 5 min at room temperature. The poly-D-lysine was then aspirated and the coverslip rinsed with DI H_2O and allowed to dry for 2 h before casting gels.

MeHA (1% wt/vol) was dissolved in 0.2 M Triethanolamine (catalog no. T58300; Sigma-Aldrich) and PBS solution. Irgacure 2959 (catalog no. 410896; Sigma-Aldrich) was dissolved at 1% wt/vol in ethanol and then diluted to 0.01% wt/vol in the MeHA solution. Fifteen microliters of the hydrogel solution was sandwiched between a poly-D-lysine–treated glass coverslip to permit hydrogel binding and a nonadherent dichlorodimethylsilane (catalog no. AC11331; Acros Organics)-activated glass slide to achieve easy detachment and photopolymerized using a transilluminator (4 mW/cm^2 at 350 nm wavelength; UVP). Initial polymerization created hydrogels of ~100–200 Pascal. Subsequent polymerization to stiffen the hydrogel depended on exposure time but ranged from 90 to 150 s, depending on the desired final

Downloaded at Palestinian Territory, occupied on November 25, 2021
www.manaraa.com

modulus using 1% wt/vol Irgacure (26). Protein for cell attachment was added by mixing 20 mM 1-ethyl-3-(3-dimethylaminopropyl) carbodiimide (catalog no. c1100; ProteoChem), 50 mM *N*-hydroxysuccinimide (catalog no. A10312; Alfa Aesar), and 150 μg/mL type I rat tail collagen (catalog no. 354236; Corning) in PBS. The collagen–cross-linker solution was added to hydrogels and incubated overnight at 37 °C.

Atomic Force Microscopy and Force Spectroscopy. Hydrogel stiffness was determined by atomic force microscopy (MFP-3D Bio; Asylum Research) with a silicon nitride cantilever (catalog no. PNP-TR; NanoAndMore USA Corporation). Materials were indented at 2 μm/s or ∼50 nN/s. Tip deflections were converted to indentation force for all samples using their respective tip spring constants and Hooke's Law. All AFM data were analyzed using custom-written code in Igor Pro (Wavemetrics) to determine Young's Modulus as previously described based on a Hertz model (39). Note that code is available at ecm.ucsd.edu/AFM.html. Protein tethering quantification by force spectroscopy was analyzed as described (27). Cantilevers were functionalized with an anti-collagen type I antibody (catalog no. C2456; Sigma) or avidin (catalog no. PRO-500; Prospec). Briefly, cantilevers were cleaned with chloroform and immersed in ethanolamine-HCl in dimethyl sulfoxide. Tips were incubated in bis(sulphosuccinimidyl)suberate (catalog no. 21580; Fisher), rinsed, and then immersed either in an antibody or avidin solution to cross-link the protein to the tip. Force curves were taken in a regular 10 × 10 array of points spaced ∼10 μm apart. To promote binding of the antibody to collagen or avidin to biotin, a dwell time of 1 s was added between approach and retraction cycles. Curves were converted to force versus tip position and then analyzed for rupture events using a previously described algorithm; rupture events were then determined.

MCF10A Assays. MCF10A cells were seeded at $10^4/cm^2$ onto MeHA hydrogels. Hydrogels were stiffened on days 2, 4, 6, 8, and 10 after seeding. Unseeded control hydrogels were tested concurrently with the AFM to determine their Young's modulus to ensure repeatable stiffening. Cell morphology was characterized by determining the percent spheroids remaining after stiffening up to 5 d after the stiffening event. For Figs. 4 and 5 and *SI Appendix*, Figs. S5 and S7–S15, compliant and stiff MeHA hydrogels were seeded with a MCF10A preformed spheroids at 250 or 500 cells per spheroid as indicated or, if not, at 250 cells per spheroid. After 2 d of culture, a subset of the compliant hydrogels was subjected to stiffening. All samples with and without Irgacure were subjected to the same UV exposure. After stiffening, the hydrogels were rinsed with 1× PBS and placed back into assay media. Morphology of the cells was observed daily, and percent spheroids remaining was determined.

Mammary spheroids were separated from spread cells using an EDTA rinse for replating onto compliant or stiff substrates to perform a secondary screen. The spread cells were removed using trypsin and seeded onto compliant and stiff substrates for an additional secondary screen. In all cases, the cells were cultured on the substrates for 2 d before the stiffening event and the percent remaining spheroids was determined.

ACKNOWLEDGMENTS. We thank Dr. Alexander Fuhrmann for assistance in calculating collagen rupture lengths and Elizabeth Bird for assistance in determining MEC substrate adhesion. Funding for this work was provided by National Institutes of Health Grants R01CA206880 (to A.J.E. and J.Y.), R21CA217735 (to A.J.E.), 1R01CA174869 (to J.Y.), F32HL126406 (to J.K.P.), and T32AR060712 (to A.K.); Department of Defense Grants W81XWH-13-1-0132 (to J.Y.) and W81XWH-13-1-0133 (to A.J.E.); National Science Foundation Grants 1463689 (to A.J.E.) and 1763139 (to A.J.E.); the Graduate Research Fellowship program (to M.G.O. and A.K.); and the Achievement Rewards for College Scientists/Roche Foundation Scholar Award Program in the Life Science (to A.K.). Additional fellowship support was provided the Brazilian Federal Agency for Support and Evaluation of Graduate Education Award 88881.135357/2016-01 (to B.F.M.).

1. Lo CM, Wang HB, Dembo M, Wang YL (2000) Cell movement is guided by the rigidity of the substrate. *Biophys J* 79:144–152.
2. Happe CL, Tenerelli KP, Gromova AK, Kolb F, Engler AJ (2017) Mechanically patterned neuromuscular junctions-in-a-dish have improved functional maturation. *Mol Biol Cell* 28:1950–1958.
3. Choi YS, et al. (2012) The alignment and fusion assembly of adipose-derived stem cells on mechanically patterned matrices. *Biomaterials* 33:6943–6951.
4. Yeung T, et al. (2005) Effects of substrate stiffness on cell morphology, cytoskeletal structure, and adhesion. *Cell Motil Cytoskeleton* 60:24–34.
5. Engler AJ, Sen S, Sweeney HL, Discher DE (2006) Matrix elasticity directs stem cell lineage specification. *Cell* 126:677–689.
6. Rowlands AS, George PA, Cooper-White JJ (2008) Directing osteogenic and myogenic differentiation of MSCs: Interplay of stiffness and adhesive ligand presentation. *Am J Physiol Cell Physiol* 295:C1037–C1044.
7. Khatiwala CB, Peyton SR, Putnam AJ (2006) Intrinsic mechanical properties of the extracellular matrix affect the behavior of pre-osteoblastic MC3T3-E1 cells. *Am J Physiol Cell Physiol* 290:C1640–C1650.
8. Lu P, Weaver VM, Werb Z (2012) The extracellular matrix: A dynamic niche in cancer progression. *J Cell Biol* 196:395–406.
9. Levental KR, et al. (2009) Matrix crosslinking forces tumor progression by enhancing integrin signaling. *Cell* 139:891–906.
10. Ng MR, Brugge JS (2009) A stiff blow from the stroma: Collagen crosslinking drives tumor progression. *Cancer Cell* 16:455–457.
11. Williams CM, Engler AJ, Slone RD, Galante LL, Schwarzbauer JE (2008) Fibronectin expression modulates mammary epithelial cell proliferation during acinar differentiation. *Cancer Res* 68:3185–3192.
12. Kao RT, Hall J, Engel L, Stern R (1984) The matrix of human breast tumor cells is mitogenic for fibroblasts. *Am J Pathol* 115:109–116.
13. Ishihara S, Inman DR, Li WJ, Ponik SM, Keely PJ (2017) Mechano-signal transduction in mesenchymal stem cells induces prosaposin secretion to drive the proliferation of breast cancer cells. *Cancer Res* 77:6179–6189.
14. Pankova D, et al. (2016) Cancer-associated fibroblasts induce a collagen cross-link switch in tumor stroma. *Mol Cancer Res* 14:287–295.
15. Wang K, et al. (2015) Stiffening and unfolding of early deposited-fibronectin increase proangiogenic factor secretion by breast cancer-associated stromal cells. *Biomaterials* 54:63–71.
16. Paszek MJ, et al. (2005) Tensional homeostasis and the malignant phenotype. *Cancer Cell* 8:241–254.
17. Wei SC, et al. (2015) Matrix stiffness drives epithelial-mesenchymal transition and tumour metastasis through a TWIST1-G3BP2 mechanotransduction pathway. *Nat Cell Biol* 17:678–688.
18. Burdick JA, Murphy WL (2012) Moving from static to dynamic complexity in hydrogel design. *Nat Commun* 3:1269.
19. Stowers RS, Allen SC, Suggs LJ (2015) Dynamic phototuning of 3D hydrogel stiffness. *Proc Natl Acad Sci USA* 112:1953–1958.
20. Burdick JA, Chung C, Jia X, Randolph MA, Langer R (2005) Controlled degradation and mechanical behavior of photopolymerized hyaluronic acid networks. *Biomacromolecules* 6:386–391.
21. Guvendiren M, Burdick JA (2012) Stiffening hydrogels to probe short- and long-term cellular responses to dynamic mechanics. *Nat Commun* 3:792.
22. Kloxin AM, Kasko AM, Salinas CN, Anseth KS (2009) Photodegradable hydrogels for dynamic tuning of physical and chemical properties. *Science* 324:59–63.
23. Tse JR, Engler AJ (2011) Stiffness gradients mimicking in vivo tissue variation regulate mesenchymal stem cell fate. *PLoS One* 6:e15978.
24. Nasrollahi S, et al. (2017) Past matrix stiffness primes epithelial cells and regulates their future collective migration through a mechanical memory. *Biomaterials* 146:146–155.
25. Yang J, et al. (2004) Twist, a master regulator of morphogenesis, plays an essential role in tumor metastasis. *Cell* 117:927–939.
26. Ondeck MG, Engler AJ (2016) Mechanical characterization of a dynamic and tunable methacrylated hyaluronic acid hydrogel. *J Biomech Eng* 138:021003.
27. Wen JH, et al. (2014) Interplay of matrix stiffness and protein tethering in stem cell differentiation. *Nat Mater* 13:979–987.
28. Berg WA, et al.; BE1 Investigators (2012) Shear-wave elastography improves the specificity of breast US: The BE1 multinational study of 939 masses. *Radiology* 262:435–449.
29. Weaver VM, et al. (1997) Reversion of the malignant phenotype of human breast cells in three-dimensional culture and in vivo by integrin blocking antibodies. *J Cell Biol* 137:231–245.
30. Panciera T, Azzolin L, Cordenonsi M, Piccolo S (2017) Mechanobiology of YAP and TAZ in physiology and disease. *Nat Rev Mol Cell Biol* 18:758–770.
31. Lin CH, et al. (2015) Microenvironment rigidity modulates responses to the HER2 receptor tyrosine kinase inhibitor lapatinib via YAP and TAZ transcription factors. *Mol Biol Cell* 26:3946–3953.
32. Wang C, et al. (2015) Verteporfin inhibits YAP function through up-regulating 14-3-3σ sequestering YAP in the cytoplasm. *Am J Cancer Res* 6:27–37.
33. Leight JL, Wozniak MA, Chen S, Lynch ML, Chen CS (2012) Matrix rigidity regulates a switch between TGF-β1-induced apoptosis and epithelial-mesenchymal transition. *Mol Biol Cell* 23:781–791.
34. Chaudhuri O, et al. (2016) Hydrogels with tunable stress relaxation regulate stem cell fate and activity. *Nat Mater* 15:326–334.
35. Kiang JD, Wen JH, del Álamo JC, Engler AJ (2013) Dynamic and reversible surface topography influences cell morphology. *J Biomed Mater Res A* 101:2313–2321.
36. Yousaf MN, Houseman BT, Mrksich M (2001) Turning on cell migration with electroactive substrates. *Angew Chem Int Ed Engl* 40:1093–1096.
37. Gillette BM, Jensen JA, Wang M, Tchao J, Sia SK (2010) Dynamic hydrogels: Switching of 3D microenvironments using two-component naturally derived extracellular matrices. *Adv Mater* 22:686–691.
38. Young JL, Kretchmer K, Ondeck MG, Zambon AC, Engler AJ (2014) Mechanosensitive kinases regulate stiffness-induced cardiomyocyte maturation. *Sci Rep* 4:6425.
39. Kaushik G, Fuhrmann A, Cammarato A, Engler AJ (2011) In situ mechanical analysis of myofibrillar perturbation and aging on soft, bilayered Drosophila myocardium. *Biophys J* 101:2629–2637.

Downloaded at Palestinian Territory, occupied on November 25, 2021

www.manaraa.com